Supplementary Information for

Chain ether-based electrolyte enables long-term continuous ammonia electrosynthesis

Shaofeng Li[1]†, Yuanyuan Zhou[1]†, Xianbiao Fu[1], Jakob B. Pedersen[1], Mattia Saccoccio[1], Suzanne Z. Andersen[1], Kasper Enemark-Rasmussen[2], Aoni Xu[1], Rokas Sažinas[1], Jon Bjarke Valbæk Mygind[1], Niklas H. Deissler[1], Jakob Kibsgaard[1], Peter C. K. Vesborg[1], Jens K. Nørskov[1]*, and Ib Chorkendorff[1]*

Corresponding authors: Jens K. Nørskov, jkno@dtu.dk; Ib Chorkendorff, ibchork@fysik.dtu.dk

†These authors contributed equally to this work

Supplementary figures

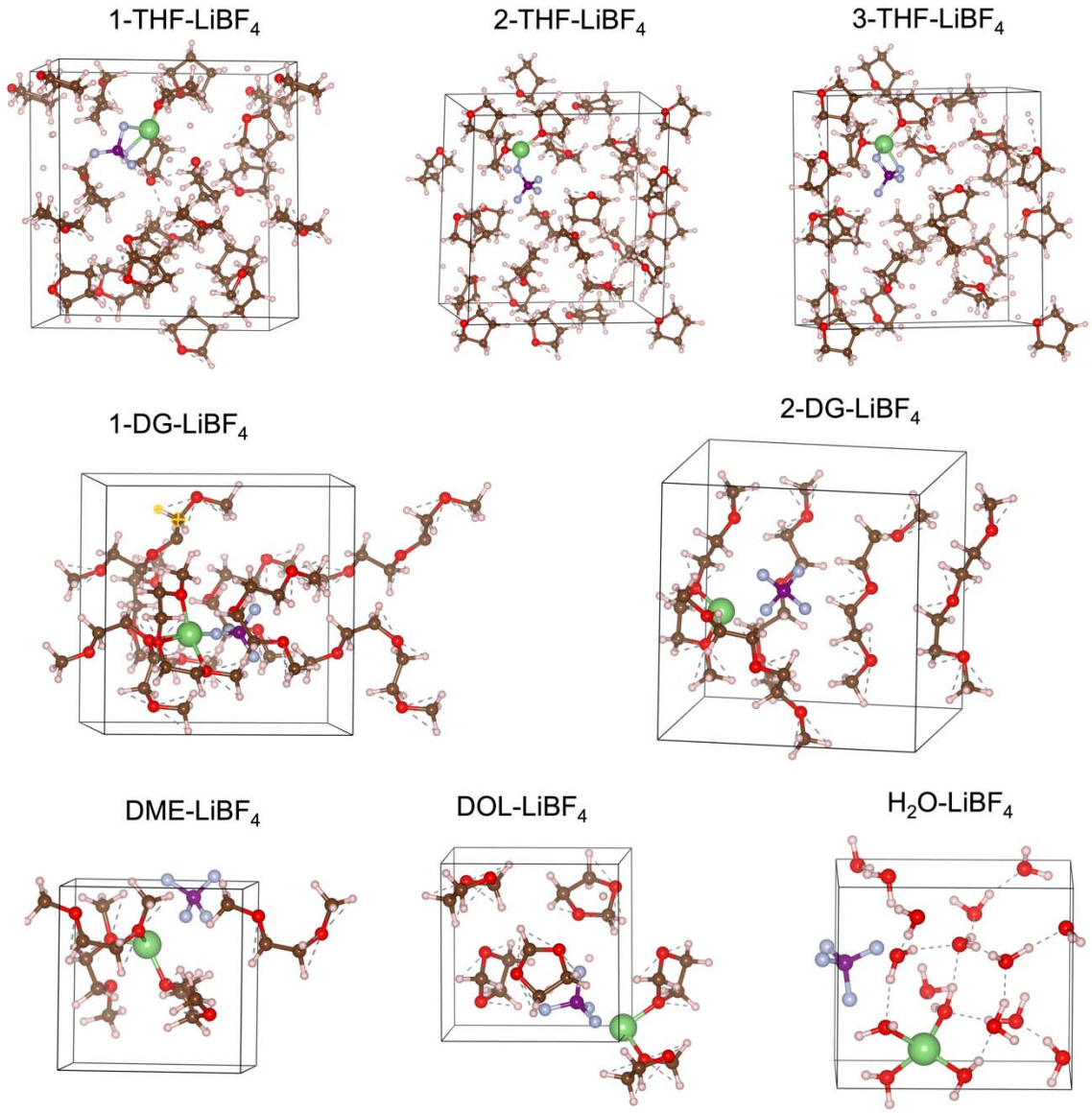

Supplementary Fig. 1 The selected $LiBF_4$ solvated conformations in the THF, DG, DME, DOL, and H_2O solvents.

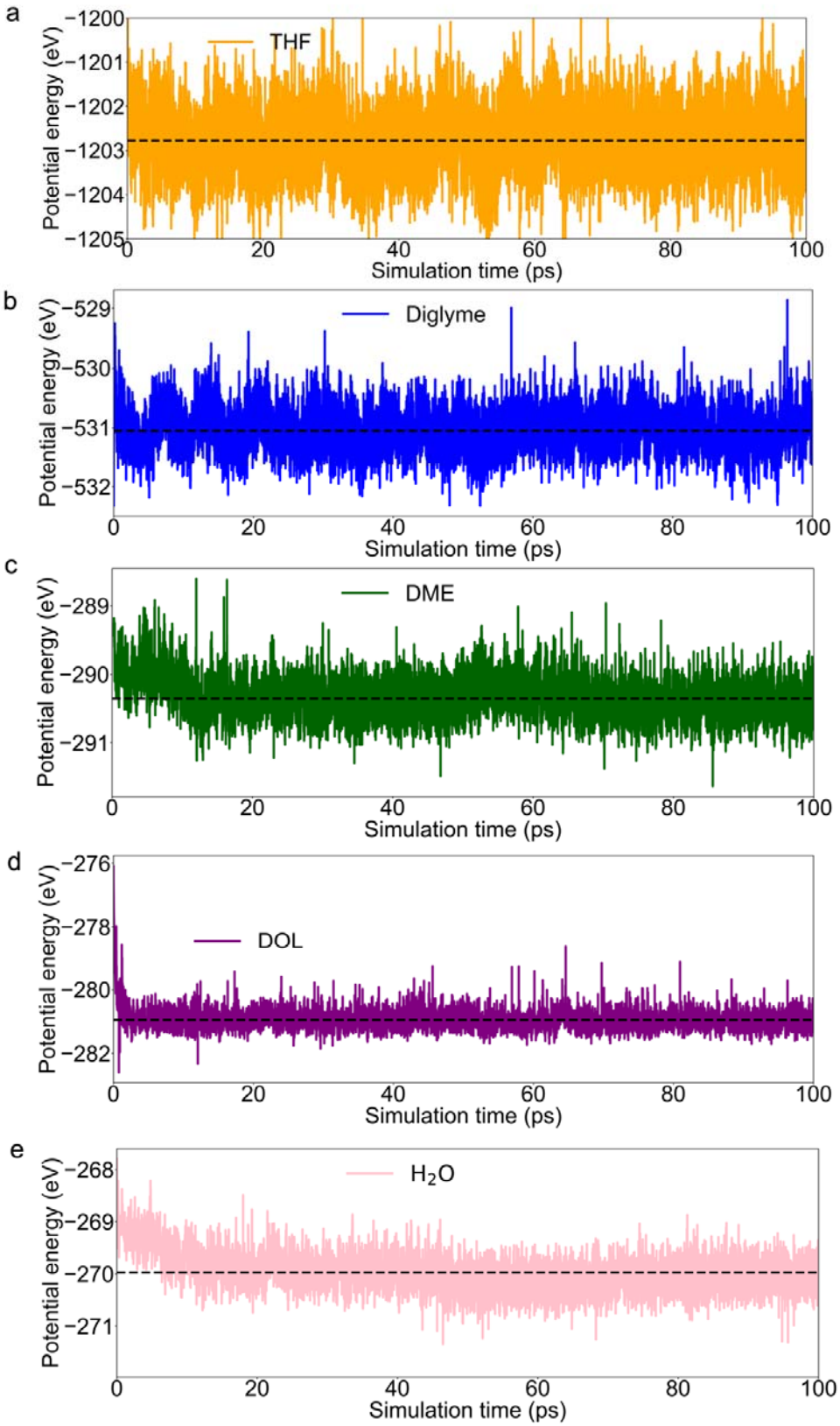

Supplementary Fig. 2 The potential energy of the $LiBF_4$ in different solvents (THF, DG, DME, DOL, and H_2O) as a function of AIMD simulation time.

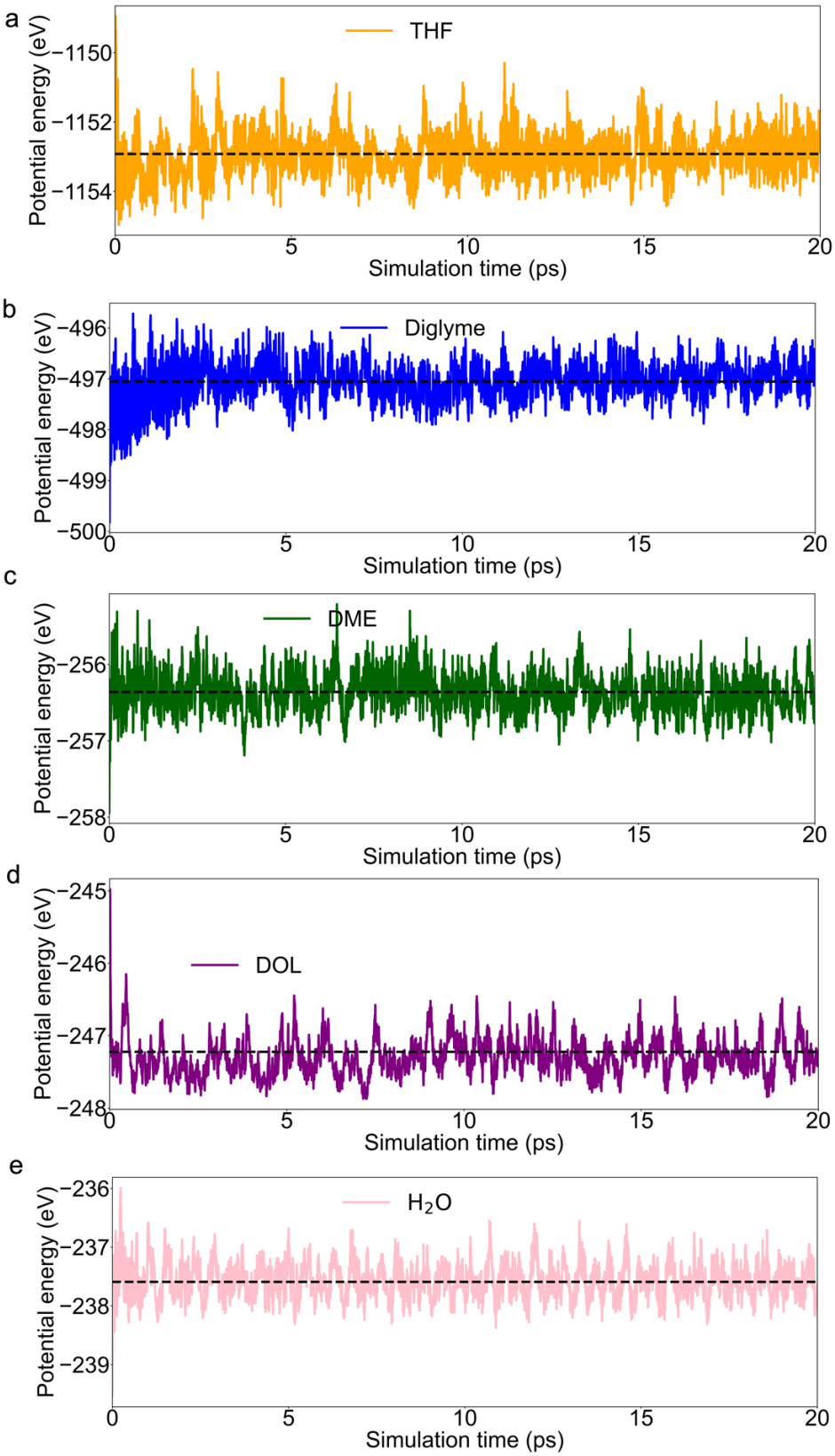

Supplementary Fig. 3 The potential energy of the pure solvents (THF, DG, DME, DOL, and H_2O) as a function of AIMD simulation time.

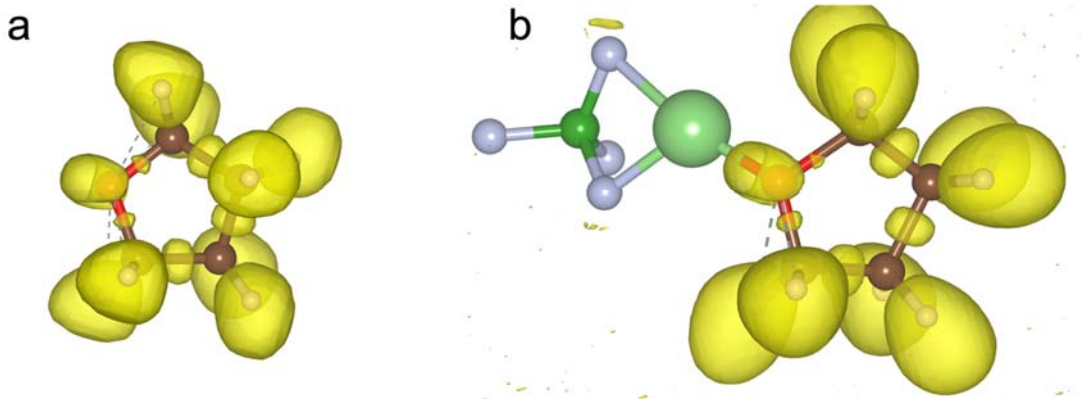

Supplementary Fig. 4 The electron localization function (ELF) of the pure THF solvent (a) and $LiBF_4$ dissolved in THF (b) at isosurface = 0.81. The ELF is calculated in the explicit model as described in the computational detail but only the relevant part is shown here.

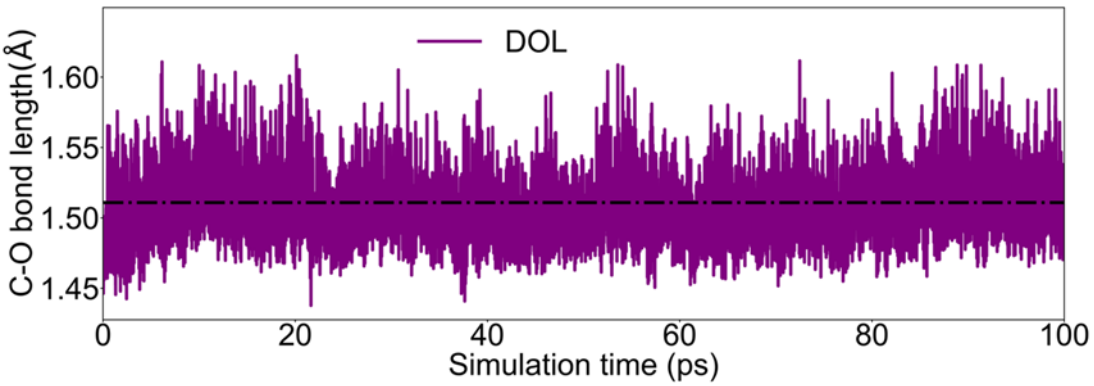

Supplementary Fig. 5 The maximum bond length of neighboring C and O atoms in the DOL solvent in the presence of $LiBF_4$.

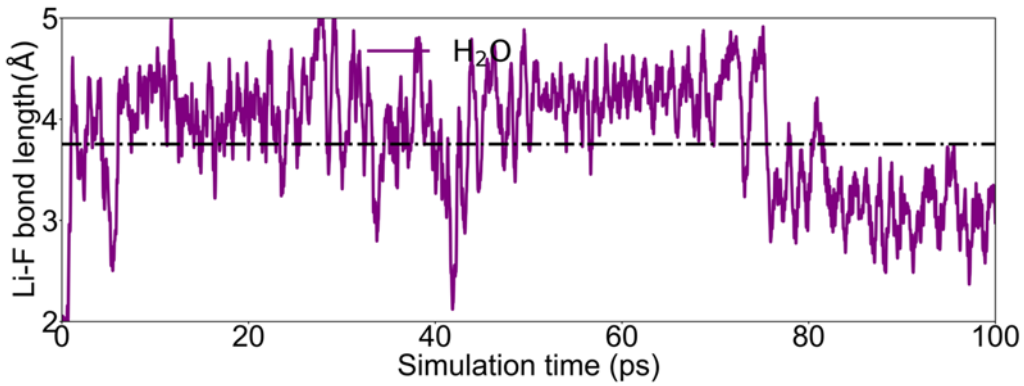

Supplementary Fig. 6 The Li and F bond length in $LiBF_4$ when dissolving H_2O during the 100 ps AIMD.

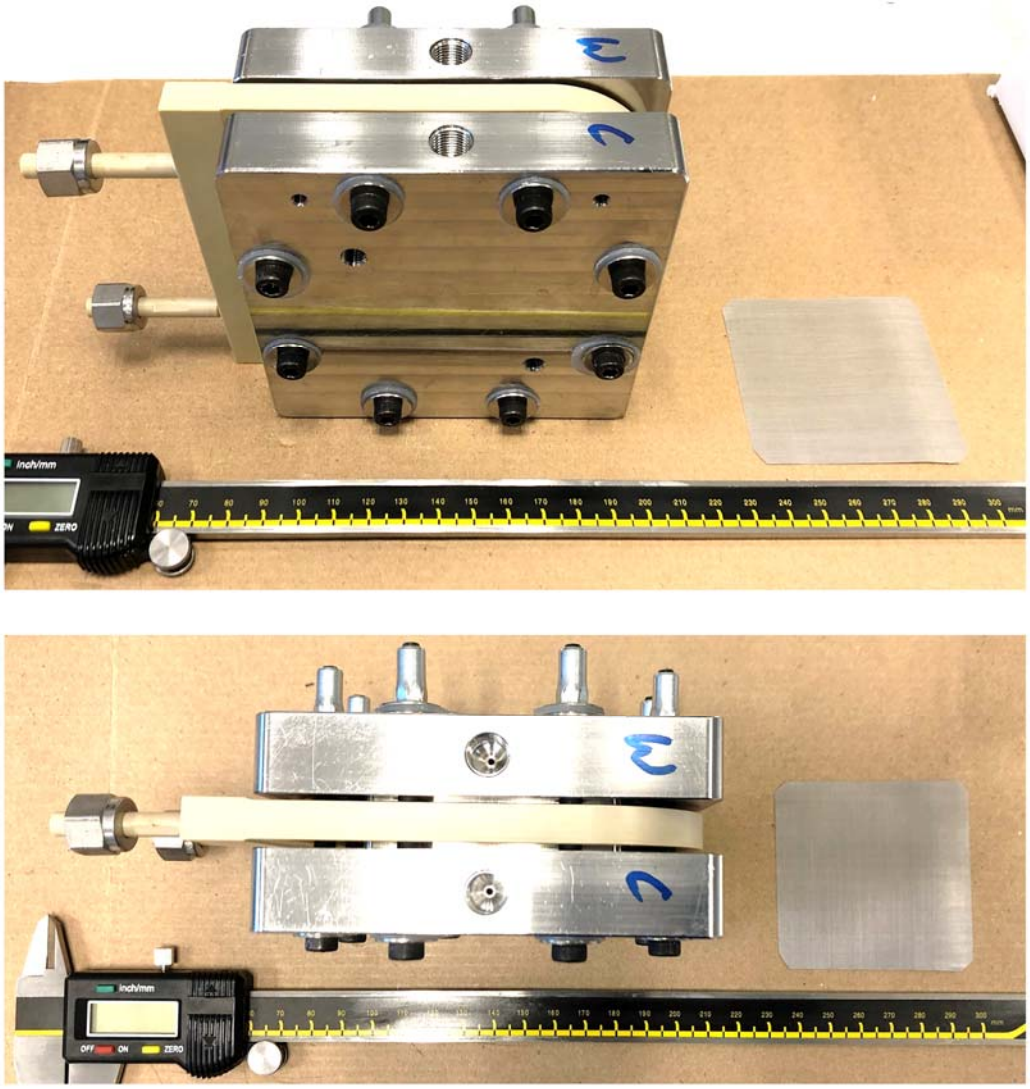

Supplementary Fig. 7 The assembled three-compartment continuous-flow reactor and working electrode for Li-NRR. The dimension of the flow cell was 10.7 cm×10.7 cm×5.1 cm. The effective area of the working electrode with gasket was 25 cm^2. The cell is compressed by bolt tightening.

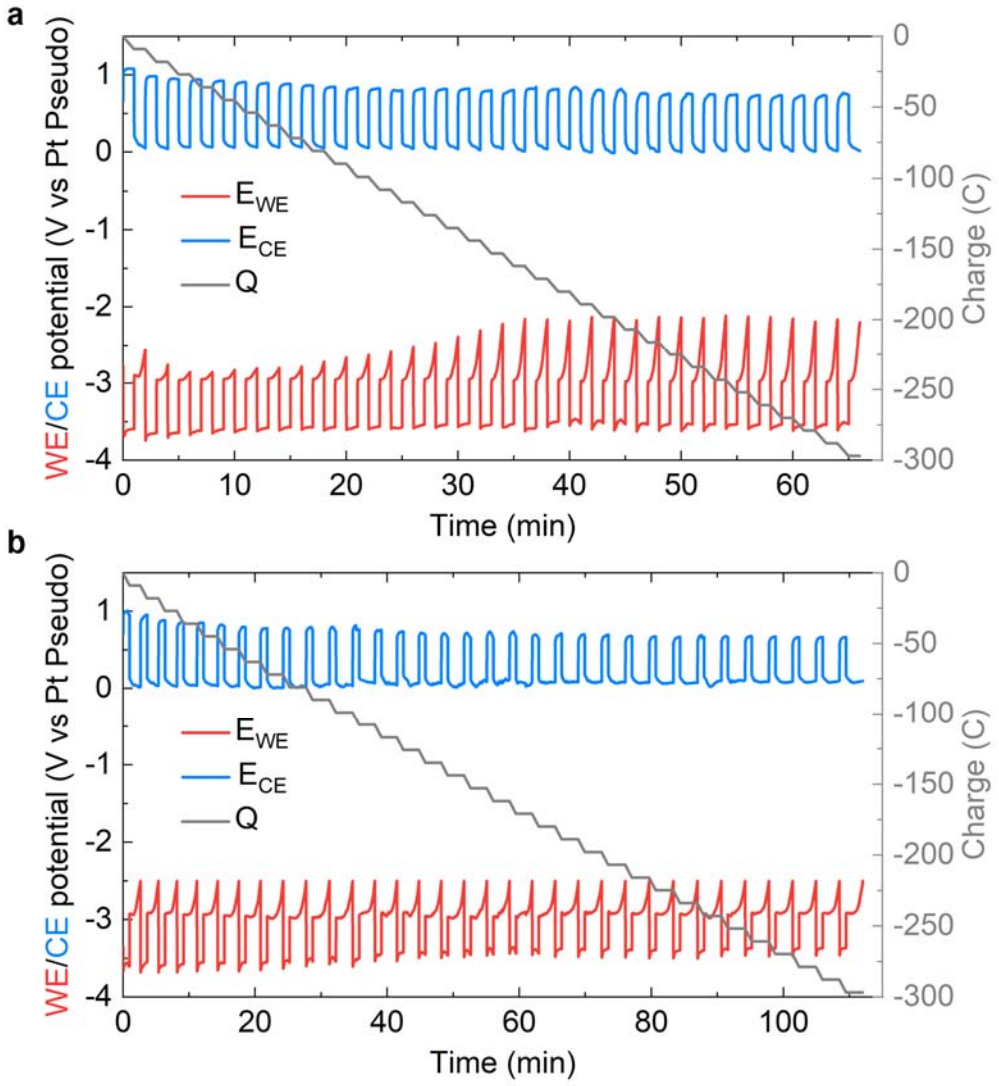

46

47 **Supplementary Fig. 8 Comparison of different cycling processes with THF. a**, 1 min for Li
48 deposition and 1 min for resting at OCV (defined as cycling in this work). **b**, 1 min for Li
49 deposition and resting until working electrode potential reach -2.5 V. All potentials are without
50 ohmic drop correction. The electrolyte is 1 M $LiBF_4$ in THF with 0.25 vol% EtOH.

51

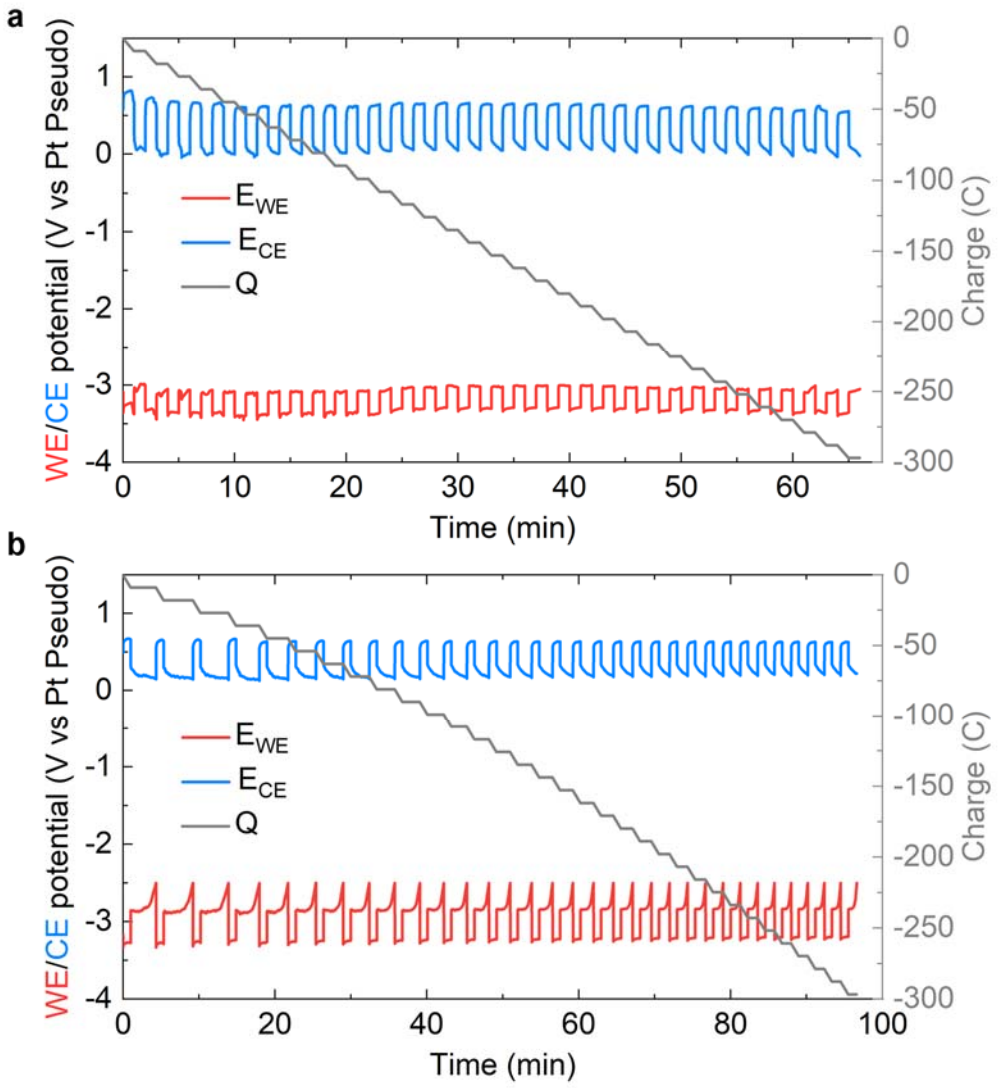

Supplementary Fig. 9 Comparison of different cycling processes with DME. a, 1 min for Li deposition and 1 min for resting at OCV (defined as cycling in this work). **b**, 1 min for Li deposition and resting until working electrode potential reach -2.5 V. All potentials are without ohmic drop correction. The electrolyte is 1 M $LiBF_4$ in DME with 0.15 vol% EtOH.

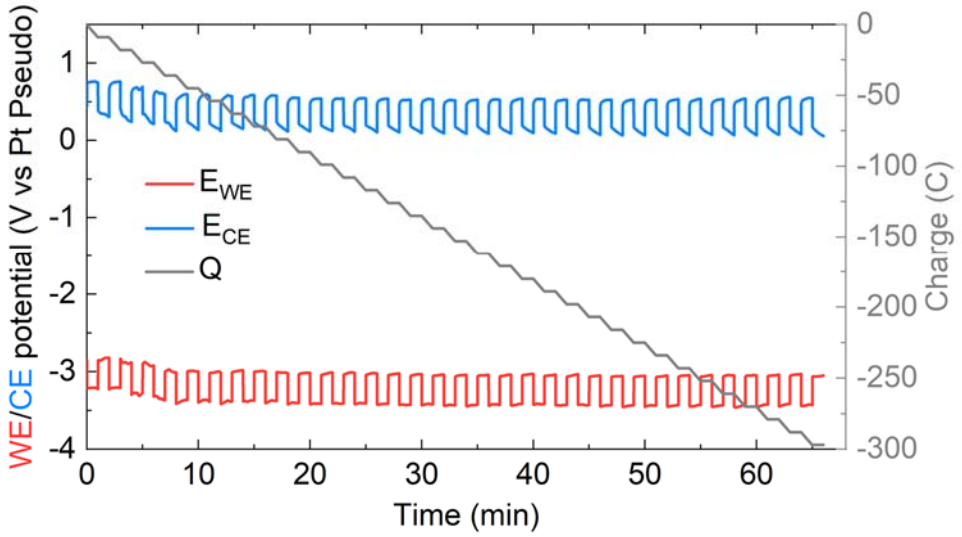

Supplementary Fig. 10 Cycling process with DG. Here the cycling process shows 1 min for Li deposition and 1 min for resting at OCV (defined as cycling in this work). All potentials are without ohmic drop correction. The electrolyte is 1 M $LiBF_4$ in DG with 0.25 vol% EtOH.

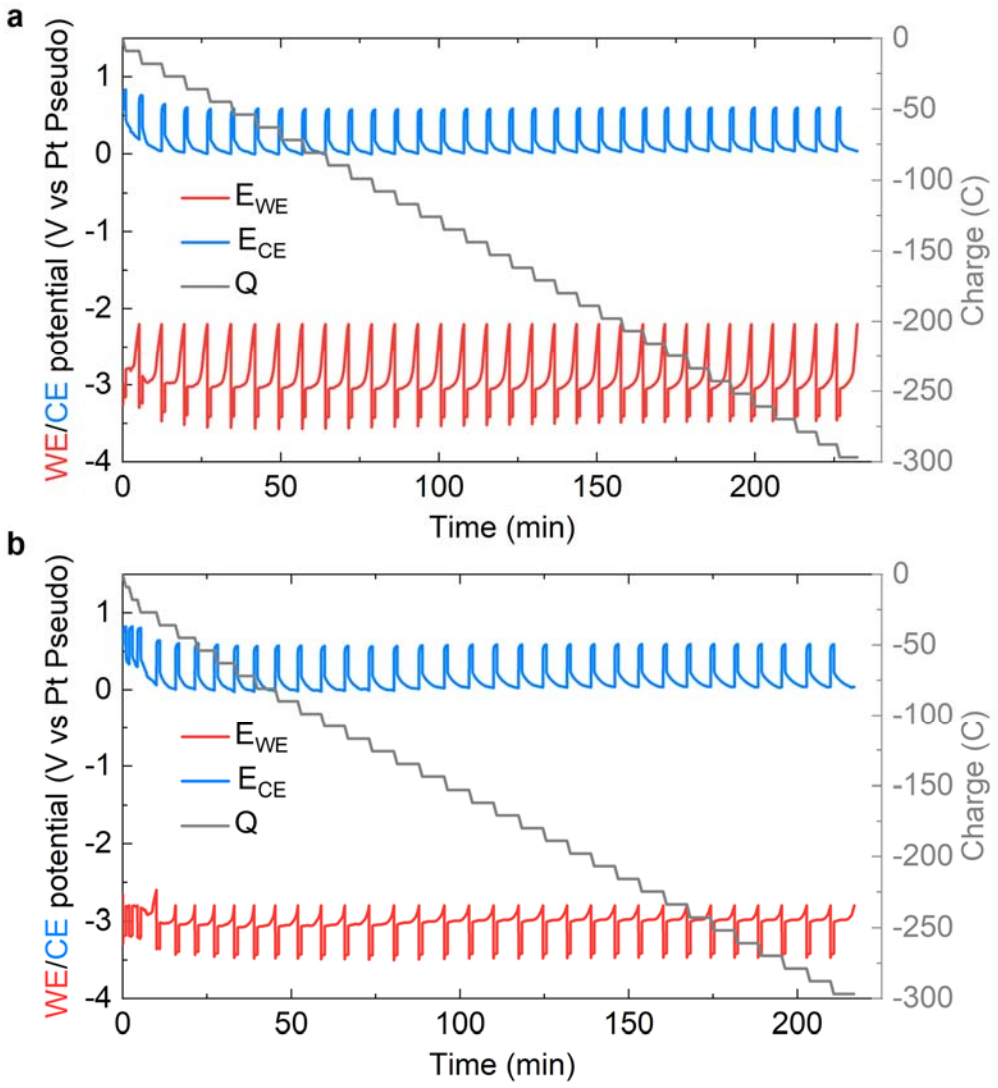

Supplementary Fig. 11 Optimizing the resting potential for the cycling process with DG. Here the cycling process shows 1 min for Li deposition and resting until working electrode potential reach -2.2 V (**a**), and -2.8 V (**b**). All potentials are without ohmic drop correction. The electrolyte is 1 M $LiBF_4$ in DG with 0.25 vol% EtOH.

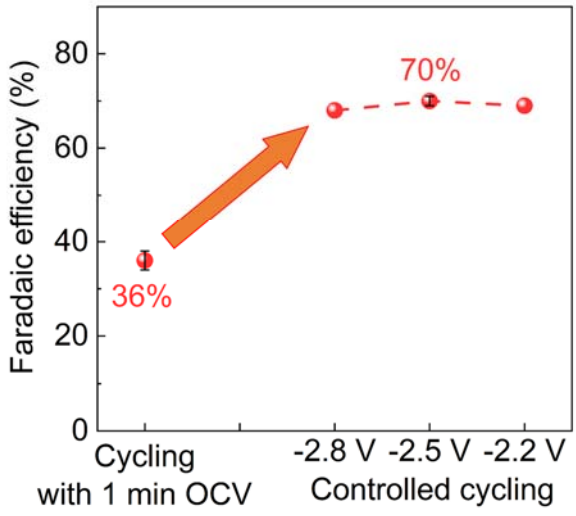

Supplementary Fig. 12 Comparison of FE with different cycling processes with DG. Cycling with 1 min OCV represents 1 min for Li deposition and 1 min for resting at OCV (defined as cycling in this work). Controlled cycling represents 1 min for Li deposition and resting until working electrode potential reach different value, e.g., -2.8, -2.5, -2.2 V.

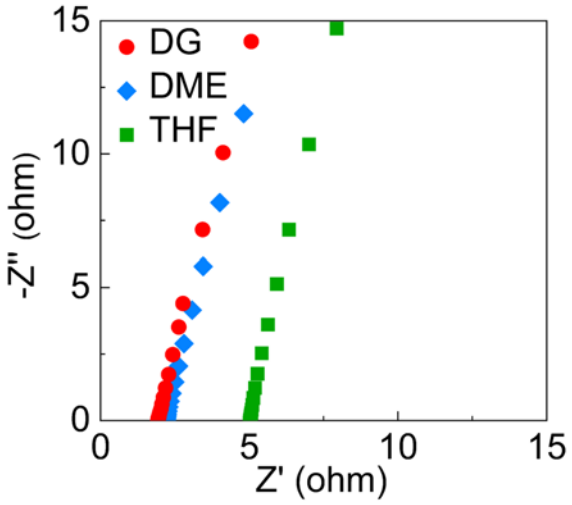

Supplementary Fig. 13 Nyquist plots of different electrolytes. The electrolyte is 1 M $LiBF_4$ in different solvents (THF, DME, DG) with 0.25 vol% EtOH.

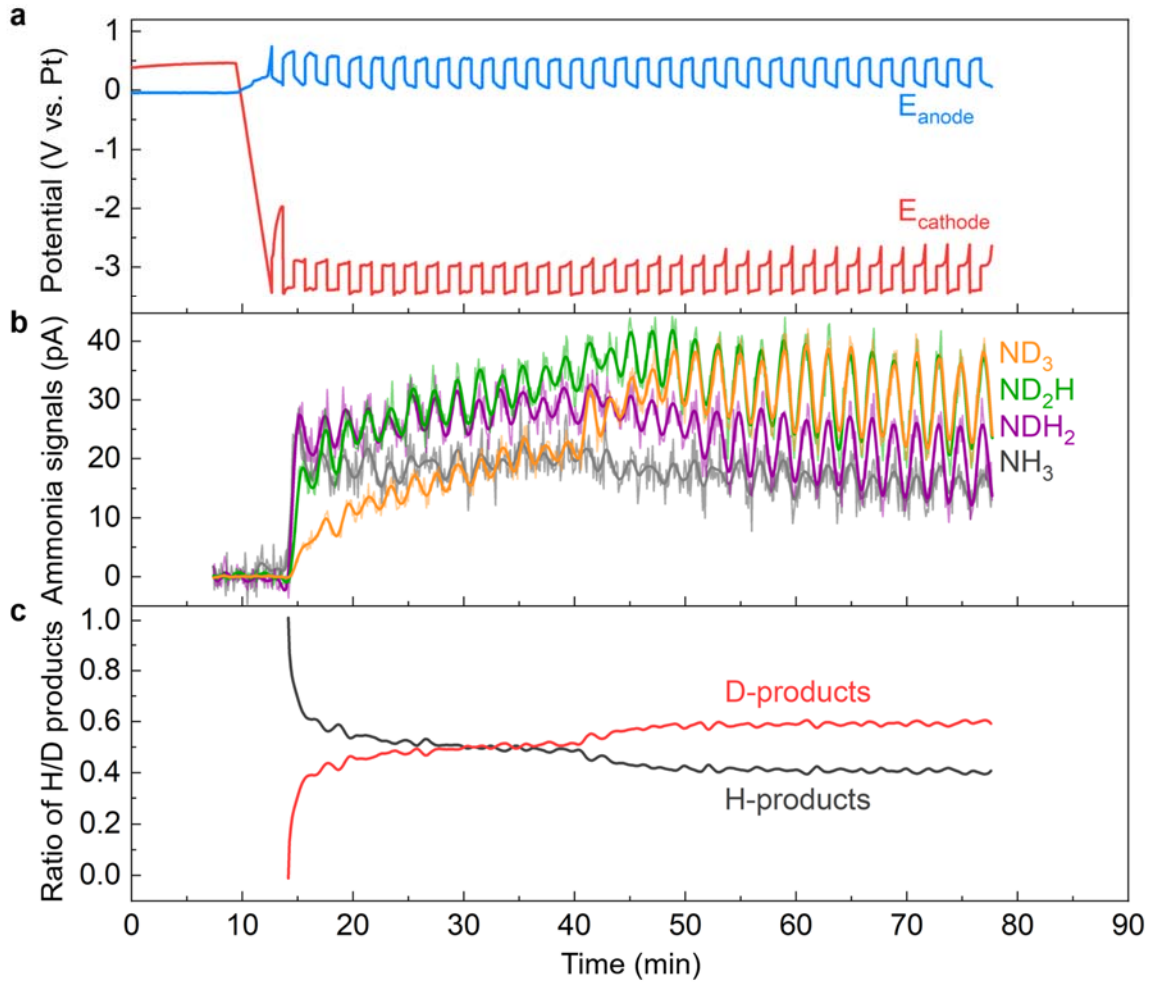

Supplementary Fig. 14 Operando mass spectrometry of cathodic ammonia gas products with isotope-labelled deuterium. a, Applied potentials during potential cycling at -6 mA/cm^2. **b**, Measured ammonia products with varying amounts of hydrogen and deuterium. **c**, Relative amounts of H and D in measured ammonia. As the experiment progresses, H is replaced with D in the proton shuttle (EtOH) leading to increased deuterated products. Here the cycling process shows 1 min for Li deposition and 1 min for resting at OCV. All potentials are without ohmic drop correction. The electrolyte is 1 M $LiBF_4$ in DME with 0.25 vol% EtOH. Initially, the cathode is fully covered in fresh electrolyte yielding mainly H-containing products, such as NH_3 and NDH_2. But as the experiment progresses, more D-containing products are formed. This unambiguously proves that coupled NRRs and HORs are occurring and demonstrates the capacity of EtOH as a proton shuttle.

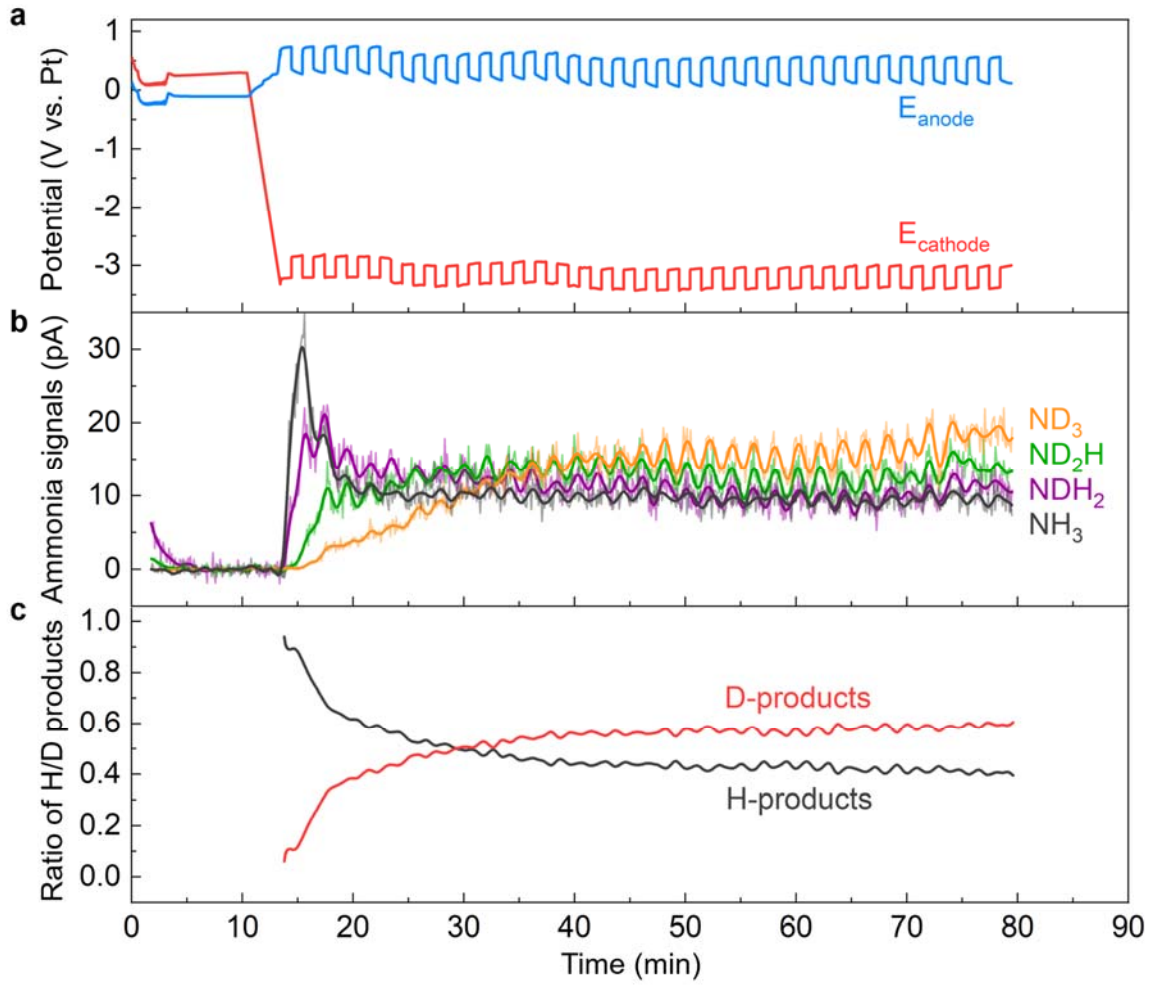

Supplementary Fig. 15 Operando mass spectrometry of cathodic ammonia gas products with isotope-labelled deuterium. a, Applied potentials during potential cycling at -6 mA/cm^2. **b**, Measured ammonia products with varying amounts of hydrogen and deuterium. **c**, Relative amounts of H and D in measured ammonia. As the experiment progresses, H is replaced with D in the proton shuttle (EtOH) leading to increased deuterated products. Here the cycling process shows 1 min for Li deposition and 1 min for resting at OCV. All potentials are without ohmic drop correction. The electrolyte is 1 M $LiBF_4$ in DG with 0.25 vol% EtOH. Initially, the cathode is fully covered in fresh electrolyte yielding mainly H-containing products, such as NH_3 and NDH_2. But as the experiment progresses, more D-containing products are formed. This unambiguously proves that coupled NRRs and HORs are occurring and demonstrates the capacity of EtOH as a proton shuttle.

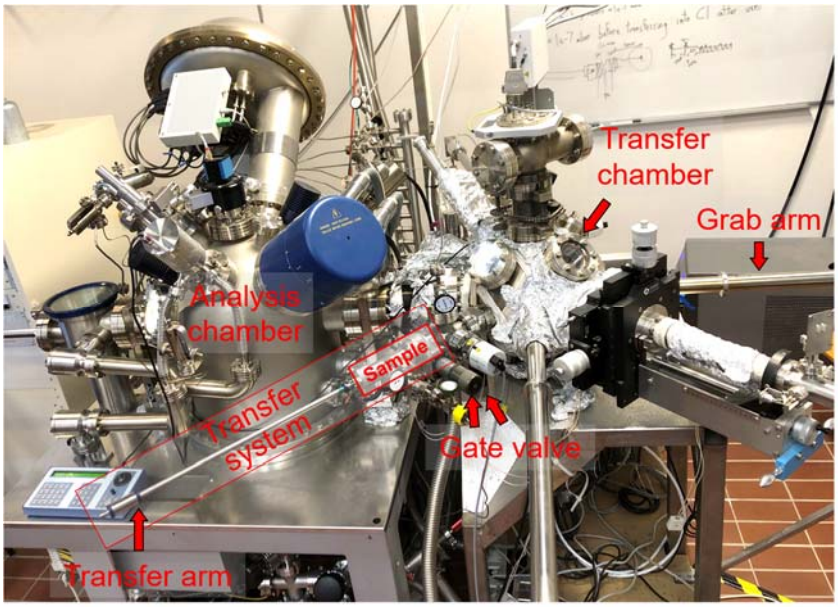

Supplementary Fig. 16 Digital photos of the home-built XPS transfer system. The transfer system was first loaded into an Ar glovebox for sample loading, and the gate valve on the system was closed. Then the system was attached to the transfer chamber and pumped down. When the pressure of the transfer system reached below 5×10^{-6} mbar, the transfer gate was opened and the sample was introduced to the transfer chamber. Finally, the grab arm is used to catch the sample and transfer it to the analysis chamber.

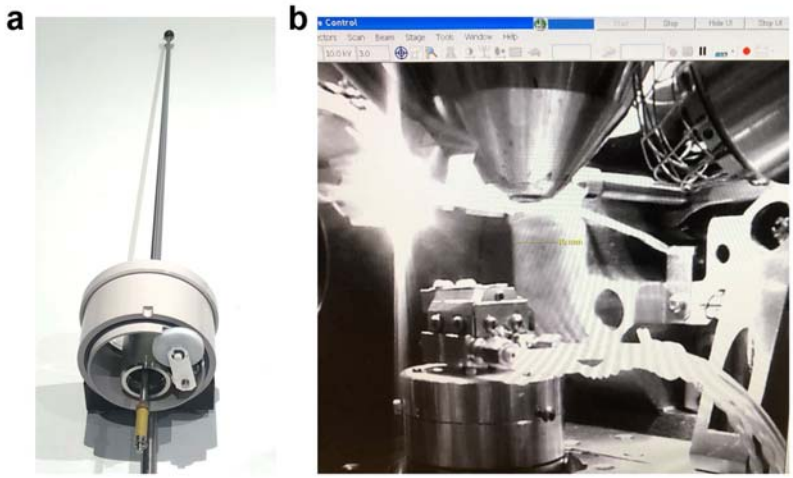

Supplementary Fig. 17 Digital photos of the SEM transfer rod. The transfer rod (**a**) was first loaded into an Ar glovebox for sample loading, and the gate valve on the rod was closed. Then the system was attached to the SEM transfer chamber and pumped down, followed by introducing the sample holder into the transfer chamber and the analysis chamber (**b**).

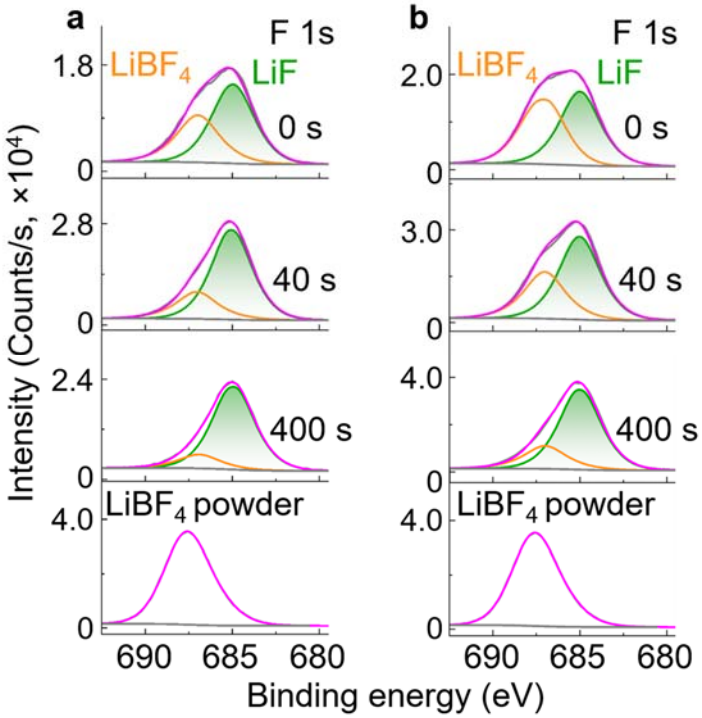

Supplementary Fig. 18 Depth-profiling XPS spectra of F 1s for the GDE using DG-based electrolyte (a) and THF-based electrolyte (b). The continuous-flow cell was run in an Ar-filled glovebox using THF and DG under the same conditions, i.e., with the passed charge of 700 C and 0.25 vol% EtOH concentration.

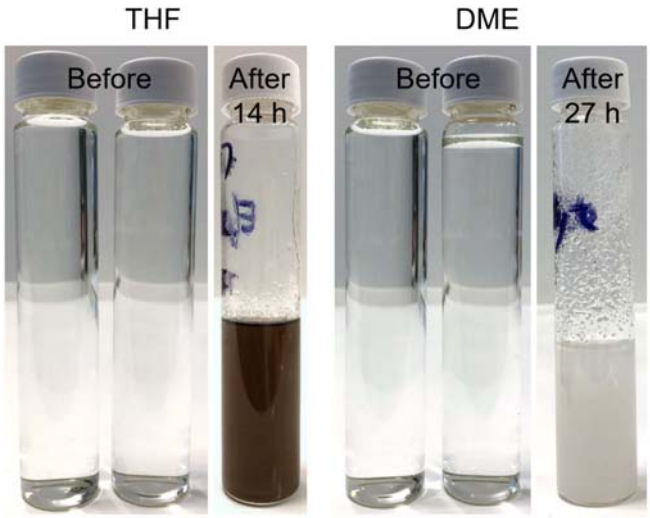

Supplementary Fig. 19 Visible change of different electrolytes before and after long-term ammonia synthesis. Before long-term ammonia synthesis, 115-120 mL of fresh electrolytes were prepared with different solvents accordingly. Specifically, 29 mL of THF-based electrolyte was left after 14 h, 27 mL of DME-based electrolyte was left after 27 h, respectively.

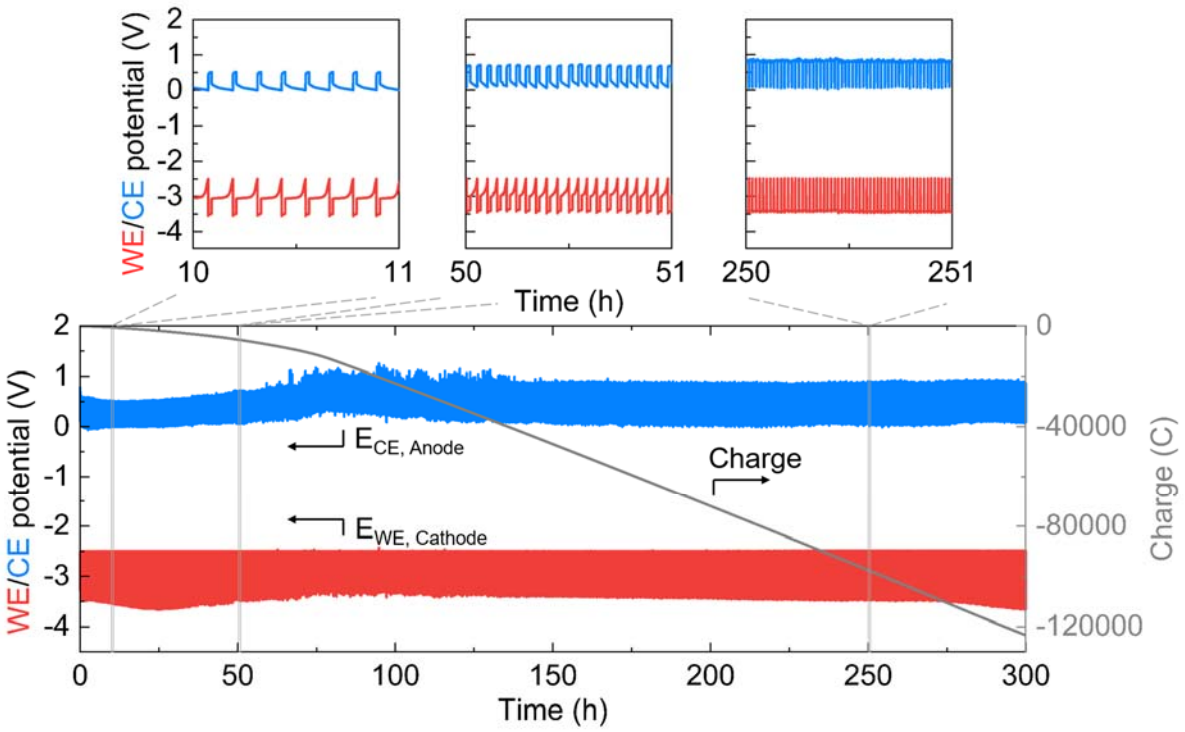

134

135 **Supplementary Fig. 20 Long-term ammonia synthesis with controlled potential cycling at -6**
136 **mA cm^{-2} using DG.** The increased rate of passed charge versus time can be ascribed to the
137 gradually reduced resting time to the resting potential (-2.5 V), which is possibly caused by water
138 content, pH and/or temperature of the electrolyte.

139

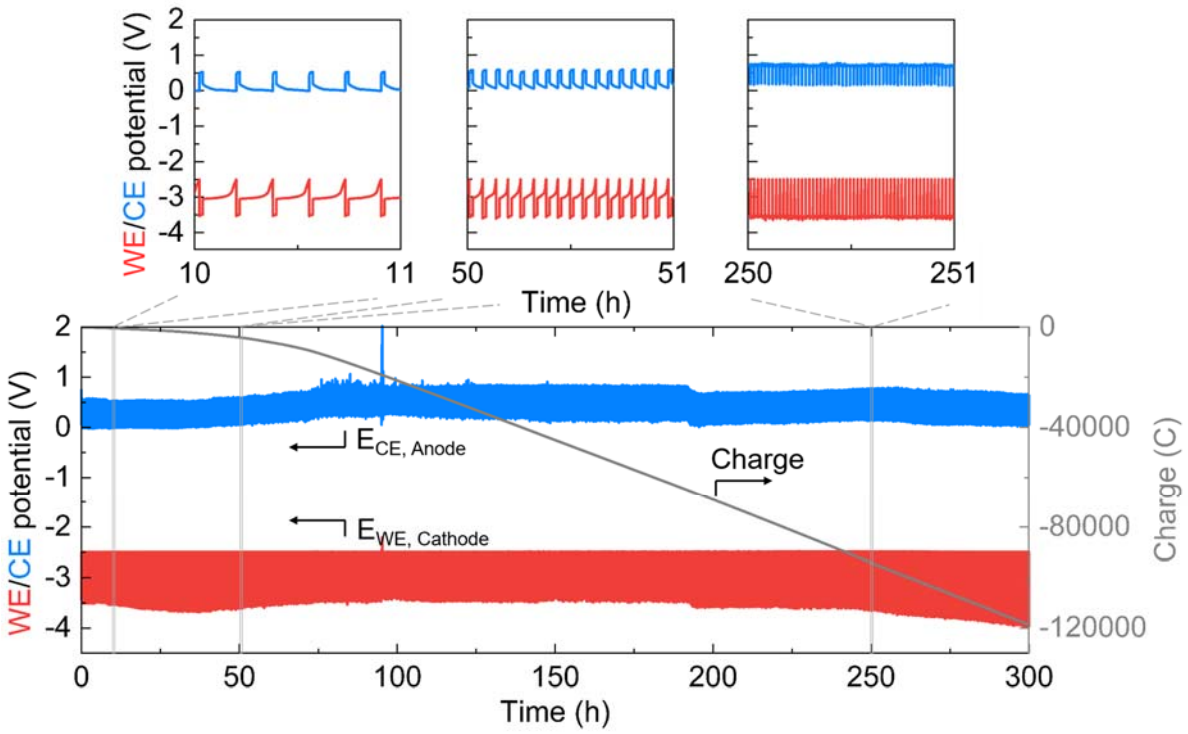

Supplementary Fig. 21 Independent long-term ammonia synthesis with controlled potential cycling at -6 mA cm^{-2} using DG. The fluctuation of the potential around 90 hours is attributed to unintentional touch during the experiment. The increased rate of passed charge versus time can be ascribed to the gradually reduced resting time to the resting potential (-2.5 V), which is possibly caused by water content, pH and/or temperature of the electrolyte.

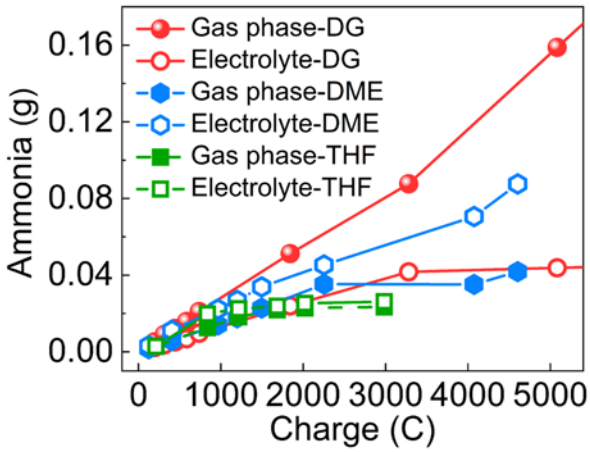

147

148 **Supplementary Fig. 22 The evolution of the ammonia distribution in gas phase and**
149 **electrolyte over passed charge for the long-term experiments using different solvents.**

150

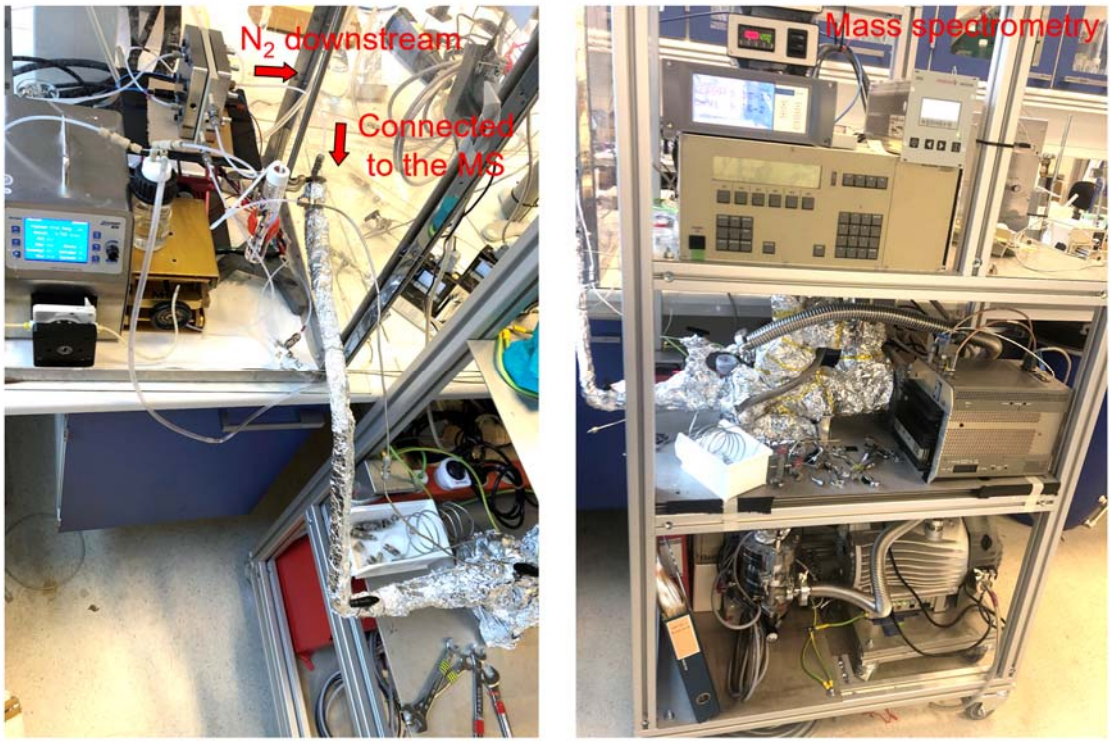

Supplementary Fig. 23 Digital photos of the home-built online mass spectrometry (MS). The MS is placed downstream on the N_2 flow from the cathode side of the flow cell. This allows for operando measurements of the flow cell operation and performance.

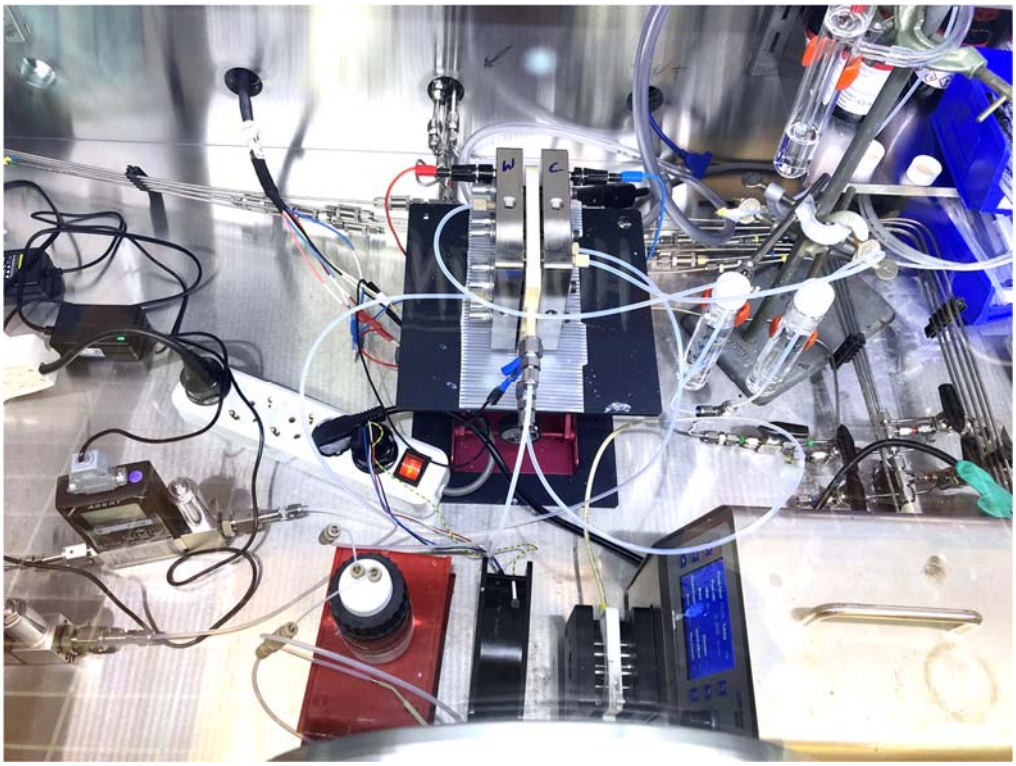

Supplementary Fig. 24 Digital photos of the flow cell experiment in an Ar-filled glovebox.

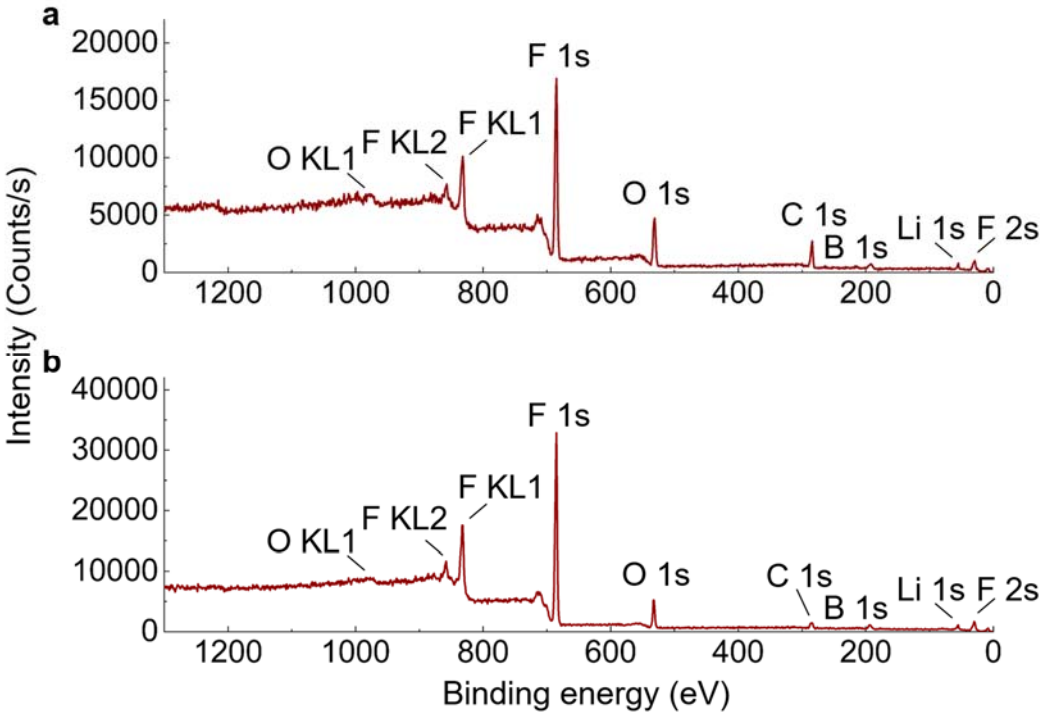

159

160 **Supplementary Fig. 25 XPS survey spectra of the GDE using DG-based electrolyte (a) and**
161 **THF-based electrolyte (b).** The continuous-flow cell was run in an Ar-filled glovebox using THF
162 and DG under the same conditions, i.e., with the passed charge of 700 C and 0.25 vol% EtOH
163 concentration.
164

Supplementary tables

Table S1. Summary of ammonia distribution in gas-phase, electrolyte, and electrode deposit for the short-term continuous ammonia electrosynthesis using different electrolyte.[*]

Solvent and cycling process	m_{NH3} (gas-phase, mg)	m_{NH3} (electrolyte, mg)	m_{NH3} (electrode deposit, mg)	m_{NH3} (total, mg)	FE (%)
THF-cycling	1.9	8.6	0.3	10.8	61.5
THF-cycling	1.9	8.4	0.3	10.6	60.6
THF-cycling	1.8	8.8	0.3	10.9	62.3
THF-controlled cycling	3.7	7.1	0.2	11.0	63.1
THF-controlled cycling	3.8	6.9	0.2	10.9	62.3
THF-controlled cycling	3.7	7.2	0.2	11.2	63.9
DME-cycling	4.5	5.0	0.2	9.7	55.3
DME-cycling	4.5	5.1	0.2	9.8	55.8
DME-cycling	4.5	4.9	0.2	9.5	54.5
DME-controlled cycling	4.8	5.1	0.2	10.1	57.6
DME-controlled cycling	5.0	5.0	0.2	10.2	58.0
DME-controlled cycling	4.6	5.2	0.2	10.0	57.1
DG-cycling	2.2	3.9	0	6.1	35.0
DG-cycling	2.2	4.0	0	6.2	35.6
DG-cycling	2.1	3.9	0	6.0	34.4
DG-controlled cycling	7.5	4.7	0	12.2	69.7
DG-controlled cycling	7.3	4.8	0	12.1	69.1
DG-controlled cycling	7.6	4.7	0	12.3	70.3

[*]The electrolyte is 1 M $LiBF_4$ in different solvents with 0.25 vol% ethanol concentrations. The passed charge for all the experiments is 297C. The cycling represents 1 min for Li deposition and 1 min for resting at OCV. The controlled cycling represents 1 min for Li deposition and resting until working electrode potential reach -2.5 V.

Table S2. Summary of the ammonia distribution in gas-phase and electrolyte for the long-term continuous ammonia electrosynthesis using THF-based electrolyte.*

Time (h)	Passed charge (C)	m_{NH3} (gas-phase, mg)	m_{NH3} (electrolyte, mg)	m_{NH3} (total, mg)	Percent of NH_3 in gas-phase (%)	Percent of NH_3 in electrolyte (%)	FE (%)
1	212	2.8	2.8	5.6	50.0	50.0	44.9
3.5	838	12.7	19.8	32.5	39.1	60.9	66.1
6	1217	18.3	22.5	40.8	44.8	55.2	57.0
9	1686	22.0	23.8	45.8	48.0	52.0	46.2
10.5	2019	22.9	25.3	48.2	47.5	52.5	40.6
14	2984	23.4	26.2	49.6	47.2	52.8	28.3

*The electrolyte is 1 M $LiBF_4$ in THF with 0.15 vol% ethanol concentrations.

Table S3. Summary of the ammonia distribution in gas-phase and electrolyte for the long-term continuous ammonia electrosynthesis using DME-based electrolyte.[*]

Time (h)	Passed charge (C)	m_{NH3} (gas-phase, mg)	m_{NH3} (electrolyte, mg)	m_{NH3} (total, mg)	Percent of NH_3 in gas-phase (%)	Percent of NH_3 in electrolyte (%)	FE (%)
2	126	1.6	3.2	4.8	33.3	66.7	64.1
4	406	5.8	11.2	17.0	34.1	65.9	71.3
7.5	964	14.0	22.3	36.3	38.6	61.4	63.9
9	1199	17.7	26.8	44.5	39.8	60.2	63.1
10.5	1496	22.8	33.9	56.7	40.2	59.8	64.4
15	2253	35.3	45.3	80.6	43.8	56.2	60.8
25	4075	35.2	70.6	116.0	30.3	69.7	48.4
27	4604	41.8	87.6	129.4	32.3	67.7	47.7

[*]The electrolyte is 1 M $LiBF_4$ in DME with 0.15 vol% ethanol concentrations.

Table S4. Summary of the ammonia distribution in gas-phase and electrolyte for the long-term continuous ammonia electrosynthesis using DG-based electrolyte in Fig. 5b and Supplementary Fig. 20.[*]

Time (h)	Passed charge (C)	m_{NH3} (gas-phase, mg)	m_{NH3} (electrolyte, mg)	m_{NH3} (total, mg)	Percent of NH_3 in gas-phase (%)	Percent of NH_3 in electrolyte (%)	FE (%)
4	198	5.2	2.2	7.4	70.3	29.7	64.1
6	315	9.0	3.7	12.7	70.9	29.1	68.5
8	446	12.3	5.2	17.5	70.3	29.7	66.5
10	584	15.8	6.8	22.6	70.0	30.0	65.9
12	737	21.0	9.7	30.7	68.4	31.6	70.8
24	1844	51.2	23.9	75.1	68.1	31.9	69.3
36	3281	87.6	41.7	129.3	67.7	32.3	67.0
48	5083	158.8	43.8	202.6	78.4	21.6	67.8
60	7479	253.0	46.1	299.1	84.6	15.4	70.0
72	10483	368.5	47.6	416.1	88.6	11.4	67.5
96	20842	760.3	50.3	810.6	93.8	6.2	66.1
108	26538	1030.8	52.1	1082.0	95.2	4.8	68.0
132	38110	1450.4	54.2	1504.6	96.4	3.6	67.1
156	49883	1892.6	58.0	1950.6	97.0	3.0	66.5
180	61857	2376.2	61.7	2437.9	97.5	2.5	70.0
204	73960	2850.3	66.6	2916.9	97.7	2.3	67.0
228	86175	3327.2	70.3	3397.5	97.9	2.1	67.0
252	98528	3734.8	73.4	3808.2	98.1	1.9	65.7
276	111065	4166.0	80.0	4246.0	98.1	1.9	65.0
300	123388	4596.8	81.6	4678.4	98.2	1.8	64.4

[*]The electrolyte is 1 M $LiBF_4$ in DG with 0.15 vol% ethanol concentrations.

Table S5. Summary of the ammonia distribution in gas-phase and electrolyte for the long-term continuous ammonia electrosynthesis using DG-based electrolyte in Supplementary Fig. 21.*

Time (h)	Passed charge (C)	m_{NH3} (gas-phase, mg)	m_{NH3} (electrolyte, mg)	m_{NH3} (total, mg)	Percent of NH_3 in gas-phase (%)	Percent of NH_3 in electrolyte (%)	FE (%)
4	180	4.8	1.8	6.6	72.7	27.3	62.1
6	261	7.3	2.2	9.5	76.8	23.2	62.3
8	351	10.3	4.1	14.4	71.5	28.5	69.9
10	441	12.3	5.3	17.6	69.9	30.1	68.2
12	549	14.8	7.1	21.9	67.6	32.4	67.9
24	1288	36.9	15.2	52.1	70.8	29.2	68.8
36	2310.3	63.2	28.5	91.7	68.9	31.1	67.5
48	3822	107.0	41.4	148.4	72.1	27.9	66.0
60	6071	190.6	42.7	233.3	81.7	18.3	65.3
72	9246	306.9	45.8	352.7	87.0	13.0	64.8
96	19426	666.3	48.8	715.1	93.2	6.8	62.6
108	25018	904.2	49.6	953.8	94.8	5.2	64.8
132	36385	1289.3	51.2	1340.5	96.2	3.8	62.6
156	47842	1718.2	56.5	1774.7	96.8	3.2	63.0
180	59285	2219.8	60.9	2280.7	97.3	2.7	65.4
204	70916	2545.9	64.6	2610.5	97.5	2.5	62.6
228	82888	3075.8	66.8	3142.6	97.9	2.1	64.4
252	95035	3532.4	70.8	3603.2	98.0	2.0	64.4
276	106832	4063.6	75.6	4139.2	98.2	1.8	65.9
300	118764	4386.0	78.2	4464.2	98.2	1.8	63.9

*The electrolyte is 1 M $LiBF_4$ in DG with 0.15 vol% ethanol concentrations.

Table S6. Summary of the stability, FEs, EEs and ammonia distribution (gas-phase and electrolyte) of previous publications and this work.

Reactor	Solvent	Stability (h)	FE (%)	EE (%)	Passed charge (C)	m_{NH3} (total, mg)	Percent of NH_3 in gas-phase (%)	Reference
Continous-flow	DG	300	64	17	123388	4678.4	98.2	This work
Continous-flow	THF	10	61	13	2600	93.0	45.0	Ref. 1
Continous-flow	THF	2.5	29.7	6.3	700	12.2	2.1	Ref. 1
Continous-flow	THF	2.5	35.1	7.4	700	14.5	47.0	Ref. 1
Continous-flow	THF	2.5	19.5	4	700	8.0	45.6	Ref. 1
Continous-flow	THF	2.5	10.8	2.2	700	4.4	24.3	Ref. 1
Continous-flow	THF	0.1	35	2.6	7	0.15	<50	Ref. 2
Batch	THF	2.0	78	11.7	50	2.3	--	Ref. 3
Batch	THF	1	24.9	3.1	12.8	0.2	--	Ref. 3
Batch	THF	2.1	20.2	1.8	27.4	0.3	--	Ref. 3
Batch	THF	0.7	18.5	1.5	7	0.1	--	Ref. 4
Batch	THF	50	37.1	6.9	100	2.2	--	Ref. 5
Batch	THF	0.8	13.6	3.9	150	1.2	--	Ref. 6
Batch	THF	93	38	8	118	2.6	--	Ref. 7
Batch	THF	96	98	15	1122	64.7	--	Ref. 8
Batch	THF	0.1	40	2.8	5	0.1	--	Ref. 9
Batch	THF	2.8	7.5	0.7	20	0.1	--	Ref. 10
Batch	THF	0.3	71	7.7	240	10.0	4.5	Ref. 11
Batch	THF	0.3	45	8.4	240	6.4	7.1	Ref. 11
Batch	THF	0.3	31	3.8	240	4.4	8.1	Ref. 11

Reference

1. Fu, X. et al. Continuous-flow electrosynthesis of ammonia by nitrogen reduction and hydrogen oxidation. *Science **379***, 707-712 (2023).
2. Lazouski, N., Chung, M., Williams, K., Gala, M.L. & Manthiram, K. Non-aqueous gas diffusion electrodes for rapid ammonia synthesis from nitrogen and water-splitting-derived hydrogen. *Nat. Catal. **3***, 463-469 (2020).
3. Li, K. et al. Enhancement of lithium-mediated ammonia synthesis by addition of oxygen. *Science **374***, 1593-1597 (2021).
4. Lazouski, N., Schiffer, Z.J., Williams, K. & Manthiram, K. Understanding continuous lithium-mediated electrochemical nitrogen reduction. *Joule **3***, 1127-1139 (2019).
5. Andersen, S.Z. et al. Increasing stability, efficiency, and fundamental understanding of lithium-mediated electrochemical nitrogen reduction. *Energy Environ. Sci. **13***, 4291-4300 (2020).
6. Li, K. et al. Increasing current density of Li-mediated ammonia synthesis with high surface area copper electrodes. *ACS Energy Lett. **7***, 36-41 (2022).
7. Suryanto, B.H. et al. Nitrogen reduction to ammonia at high efficiency and rates based on a phosphonium proton shuttle. *Science **372***, 1187-1191 (2021).
8. Du, H.-L. et al. Electroreduction of nitrogen with almost 100% current-to-ammonia efficiency. *Nature **609***, 722-727 (2022).
9. Cai, X. et al. Lithium-mediated electrochemical nitrogen reduction: mechanistic insights to enhance performance. *iScience **24***, 103105 (2021).
10. Andersen, S.Z. et al. A rigorous electrochemical ammonia synthesis protocol with quantitative isotope measurements. *Nature **570***, 504-508 (2019).
11. Li, S. et al. Electrosynthesis of ammonia with high selectivity and high rates via engineering of the solid-electrolyte interphase. *Joule **6***, 2083-2101 (2022).